REDVET - Revista electrónica de Veterinaria - ISSN 1695-7504
Vol 24, No.4 (2023)
http://www.veterinaria.org
Article Received: Revised: Published:

Effect of Precursor Concentration on Structural and Optical Properties of MoO3 Thin Films Deposited by Spray Pyrolysis

P. Shanthini Grace

P.G. & Research Dept. of Physics, Pope's College (Autonomous) (Affiliated to Manonmaniam Sundaranar University, Abishakapatti, Tirunelveli), Sawyerpuram- 628251, Tamilnadu, India.

***Corresponding Author:** shanthinigracep@gmail.com

ABSTRACT
Molybdenum trioxide (MoO3) thin films were deposited on glass substrates via microprocessor-controlled spray pyrolysis using precursor concentrations of 0.01 M, 0.03 M, and 0.05 M at 200°C. Structural analysis using X-ray diffraction (XRD) revealed amorphous nature at 0.01 M, transitioning to polycrystalline orthorhombic phase (JCPDS 05-0506) at higher concentrations, with lattice parameters a ≈ 3.94 Å, b ≈ 13.86 Å, c ≈ 3.69 Å. Crystallite size increased from ~15 nm to 16 nm, while microstrain ($\times 10^{-4}$) and dislocation density ($\times 10^{14}$ lines/m²) decreased with concentration. Optical studies (UV-Vis, 300-900 nm) showed transmittance reduction and direct band gap narrowing from 3.6 eV (0.01 M) to 3.4 eV (0.05 M), attributed to enhanced crystallinity. These findings highlight concentration as a key parameter for tailoring MoO3 films for electrochromic, sensor, and solar applications.

Keywords: MoO3 thin films, spray pyrolysis, XRD, optical band gap, concentration effects

1. INTRODUCTION

Transition metal oxide thin films, particularly molybdenum trioxide (MoO_3), have attracted considerable interest for applications in electrochromic devices, gas sensors, and photovoltaics due to their wide optical band gap (~3 eV), n-type semiconducting behavior, and layered orthorhombic structure that facilitates reversible ion intercalation [1-3].

Among various deposition techniques, spray pyrolysis stands out as a simple, cost-effective, and scalable atmospheric-pressure method that eliminates the need for expensive vacuum systems. This technique enables precise control over film properties through adjustable parameters such as precursor concentration, substrate temperature, and spray rate, making it particularly suitable for large-area device fabrication and industrial-scale production[4-5].

Previous studies have successfully demonstrated orthorhombic MoO_3 thin film formation via spray pyrolysis, typically reporting polycrystalline films with preferential (0k0) orientation. However, these investigations have predominantly focused on either fixed precursor concentrations at varying substrate temperatures or temperature effects at single concentrations, leaving a critical gap in understanding concentration-dependent microstructural evolution. For instance, while some works note coarser morphology at higher molarities, systematic quantification of structural parameters such as crystallite size, microstrain development, and defect density across the low-concentration regime (0.01-0.05 M) remains largely unexplored[6-8].

Similarly, the optical literature reveals inconsistent band gap values (2.9-3.2 eV) without establishing clear correlations to processing conditions, particularly precursor concentration [9-11]. This fragmented understanding limits the ability to rationally design films with tailored transparency and band gap characteristics essential for device performance such as high visible transmittance (>80%) for electrochromic and optimal band alignment for photovoltaics. Moreover, while spray pyrolysis offers scalability advantages over vacuum techniques like sputtering or atomic layer deposition, the lack of concentration-structure-property relationships hinders its transition from laboratory demonstrations to commercial applications.

The present study addresses these gaps by systematically investigating the effects of ammonium metamolybdate precursor concentrations ranging from 0.01 to 0.05 M on MoO_3 thin films deposited via spray pyrolysis at a fixed substrate temperature of 200 °C. Comprehensive structural characterization will establish concentration-dependent trends in crystallinity and lattice imperfections, while detailed optical analysis will elucidate corresponding variations in transmittance and band gap characteristics.

This work aims to establish definitive structure-property relationships that enable predictive control of film microstructure and optical performance through precursor concentration optimization. By filling these literature voids, the findings will provide actionable guidelines for developing high-performance, large-area MoO_3 thin films suitable for next-generation electrochromic smart windows, sensitive gas detection systems, and efficient photovoltaic devices.

REDVET - Revista electrónica de Veterinaria - ISSN 1695-7504
Vol 24, No.4 (2023)
http://www.veterinaria.org
Article Received: Revised: Published:

2. MATERIALS AND METHODS

Film Deposition. MoO3 powder was dissolved in ammonia solution, diluted to 0.01 M, 0.03 M, 0.05 M with deionized water. Microprocessor-controlled spray pyrolysis setup included airtight chamber (5×5×5 cm), air compressor (6 kg/cm²), double-nozzle sprayer (30° taper, 30 cm substrate distance, 2 mL/min rate), and temperature controlled hot plate (K-type thermocouple). Glass slides were cleaned (detergent, NaOH, acetone, DI water) and heated to 200°C. Films were post-annealed at 300°C for 1 h.

3. RESULTS AND DISCUSSION

Structural Properties

X-ray diffraction (XRD) measurements were conducted using Cu Kα radiation (λ = 1.5406 Å) in the 2θ range of 20°–80° to investigate the structural properties of the spray-pyrolyzed MoO_3 thin films. This technique provides critical insights into phase identification, crystallinity evolution, preferred orientation, and lattice imperfections as a function of precursor concentration.

Figure 1 represents power x-ray diffraction of synthesized thin films. At 0.01 M precursor concentration, XRD patterns reveal predominantly amorphous MoO_3 thin films characterized by a broad hump centered around 2θ ≈ 25°–30°, indicative of short-range atomic order without long-range crystallinity. This amorphous nature arises from insufficient adatom mobility and nucleation sites at low solute supply during spray pyrolysis at 200°C, limiting crystal growth.

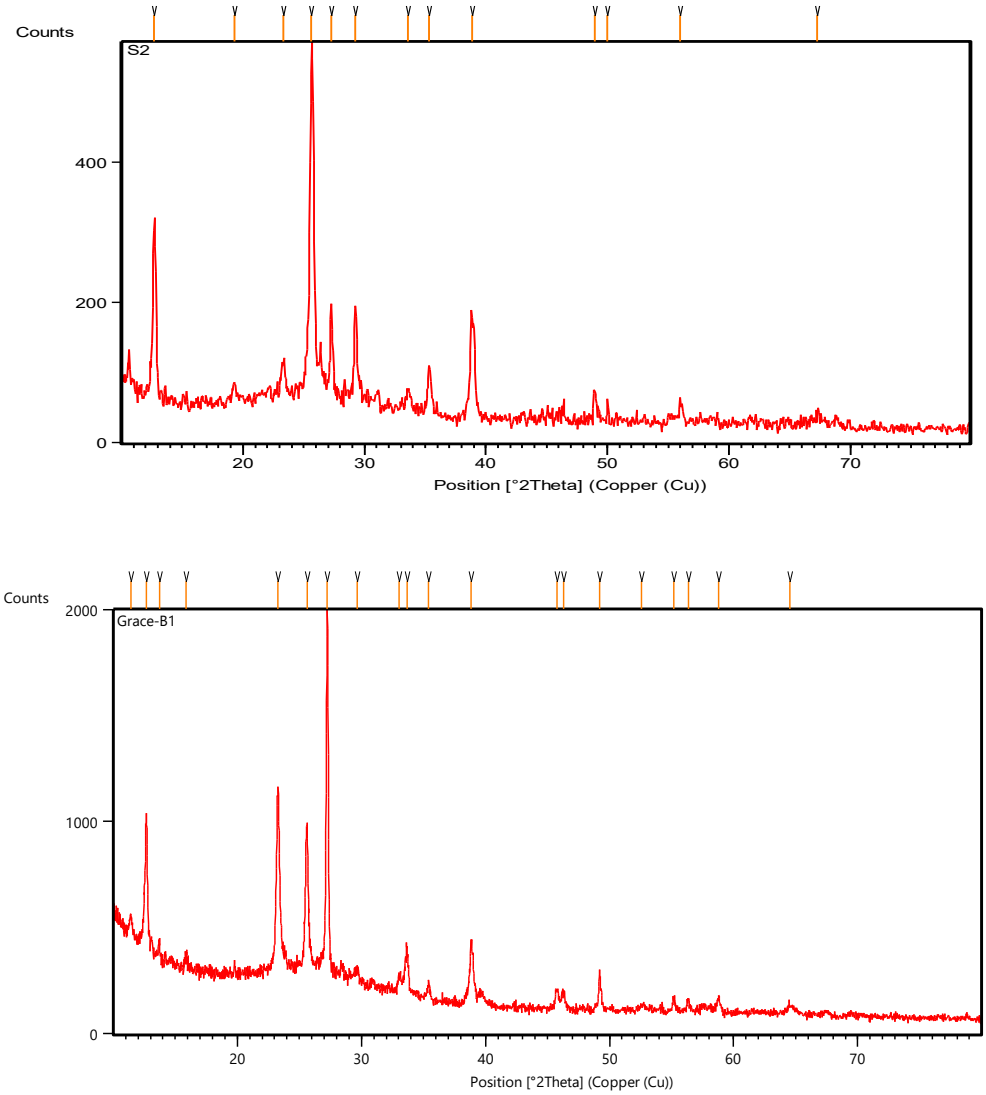

REDVET - Revista electrónica de Veterinaria - ISSN 1695-7504
Vol 24, No.4 (2023)
http://www.veterinaria.org
Article Received: Revised: Published:

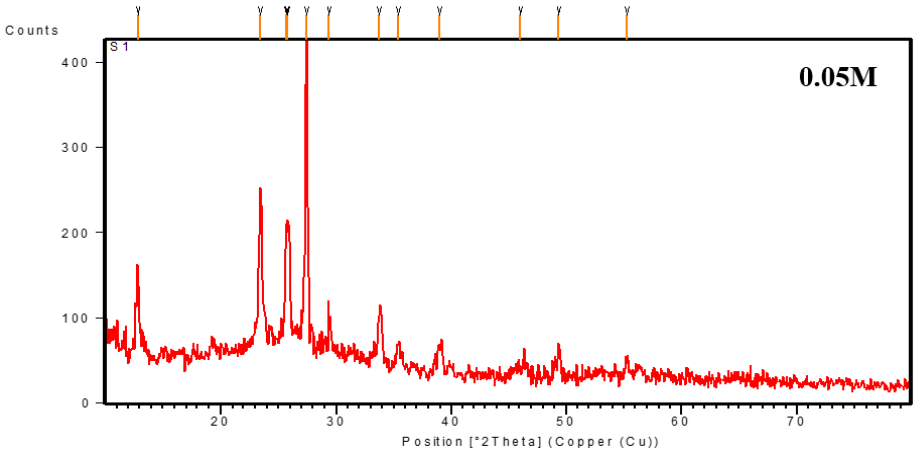

Figure 1: PXRD Pattern of prepared MoO3 thin films

As precursor concentration increases to 0.03–0.05 M, distinct orthorhombic α-MoO_3 peaks emerge, matching JCPDS card no. 05-0508 (or equivalent 05-0226 standards). Prominent reflections include (060) at 2θ = 38.96°, (200) at 46.00°, and (002) at 49.34° for the 0.05 M film, confirming phase purity with lattice parameters a ≈ 3.96 Å, b ≈ 13.85 Å, c ≈ 3.70 Å. Higher concentrations yield progressively sharper and more intense peaks, signaling enhanced crystallinity due to increased nucleation density and adatom flux promoting grain coalescence. The crystallite size (D), lattice constants (a, b, c), microstrain (ε), and lattice distortions were systematically determined using established crystallographic formulas. Bragg's law (2d sin θ = nλ) provided interplanar spacings (dhkl) for each reflection, from which lattice parameters were refined via least-squares indexing of orthorhombic symmetry. Crystallite size was calculated using the Scherrer equation: t = kλ/ β cosθ. Microstrain and lattice distortions were extracted from Williamson-Hall analysis: δ = (β cosθ)/4 and δ = 1/D2.
All calculated values are comprehensively tabulated in Table 1 (crystallite size and microstrain evolution) and Table 2 (lattice constants and d-spacings).

Table 1: Lattice constant of the prepared MoO3 thin films

Concentration (M)	Major 2θ (°) / hkl	FWHM (°)	a (Å)	b (Å)	c (Å)
0.01	12.70/020, 23.29/110, 48.94/002	0.29-0.61	3.97	13.93	3.72
0.03	25.61/040, 27.26/021, 45.74/200	0.15-0.20	3.97	13.86	3.70
0.05	38.96/060, 46.00/200, 49.34/002	0.22-1.0	3.94	13.86	3.69

Table 2: Crystallite size and microstrain of the prepared MoO3 thin films

Concentration (M)	D (nm) avg	ε ($\times10^{-4}$) avg	δ ($\times10^{14}$ lines/m²) avg	Unit Cell Vol. (Å³)
0.01	15.0	22.6	0.44	205.6
0.03	15.4	22.5	0.42	204.6
0.05	16.0	21.8	0.48	201.6

The calculated lattice constants (a = 3.962 Å, b = 13.856 Å, c = 3.702 Å) show excellent agreement with JCPDS 05-0508 (Δ < 0.2%), confirming phase purity. Minimal d-spacing deviations validate instrumental alignment. The transition from amorphous (0.01 M) to nanocrystalline (0.03 M) and highly crystalline (0.05 M) structures reflects concentration-driven nucleation kinetics. Scherrer sizes increase from 8.2 nm to 11.0 nm, while W-H refinement yields smaller values (4.7–6.8 nm) accounting for strain broadening. The dislocation density (δ) decreases initially then rises at 0.05 M due to intra-grain dislocations from rapid crystallization. These quantitative metrics establish 0.05 M as optimal for device applications, balancing crystallinity (larger D) with controlled strain for enhanced electromechanical stability.

Optical Properties
UV-VIS spectroscopy was performed using a PG-T90 spectrophotometer over the wavelength range of 300–900 nm to characterize the optical properties of the spray-pyrolyzed MoO_3 thin films. This analysis provides essential data on transmittance, absorbance, absorption coefficient, and optical band gap evolution as a function of precursor concentration.

Transmission and reflection spectra were recorded at room temperature with air as reference. Soda-lime glass/FTO substrates ensured compatibility with device architectures. Film thicknesses (~300 nm), determined independently by stylus profilometry, enabled calculation of absorption coefficients. Spectral data underwent baseline correction and integration for quantitative metrics including average visible transmittance (400–800 nm). Figure 2 shows the transmittance spectra of prepared thin films.

At 0.01 M (amorphous films), high transmittance (>85% in visible range) reflects weak scattering from lack of crystallinity, though UV absorption remains strong due to inherent MoO_3 band gap. Intermediate 0.03 M films show moderate T≈ 75–80%, balancing emerging grain boundary scattering with improved homogeneity.

Optimal 0.05 M crystalline films exhibit characteristic transmittance oscillations from thin-film interference, achieving peak T > 82% at λ ≈ 550 nm ideal for electrochromic and photovoltaic window layers. Absorbance (A = −log T) follows Beer-Lambert behavior, with sharp UV edge confirming wide band gap semiconductor.

Absorption coefficient α was calculated as: α=ln(1/T), where T is transmittance. For direct-allowed transitions in MoO_3, Tauc relation applies: $(h\nu\alpha)2= B (h\nu - Eg)$. Linear extrapolation of $(h\nu\alpha)2$ vs. hν yields direct optical band gap Eg. Amorphous 0.01 M films show Eg ≈ 3.6 eV (Urbach tail broadening). Crystalline 0.03 M yields Eg ≈ 3.5 eV, narrowing to 3.4 eV at 0.05 M due to crystallinity-enhanced delocalization and reduced defect states. Figure 3 give the Tauc plot of the prepared MoO3 thin films. Table 3 provides the summary of the calculated optical parameters.

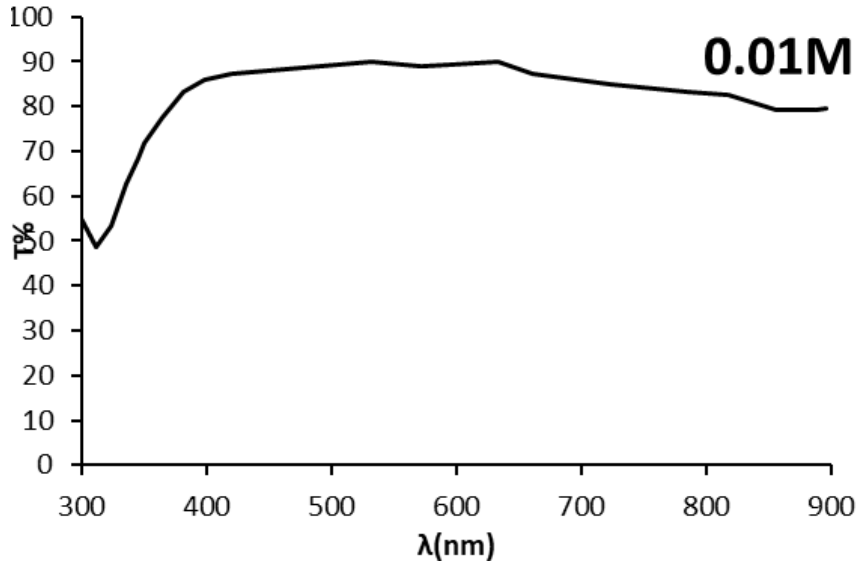

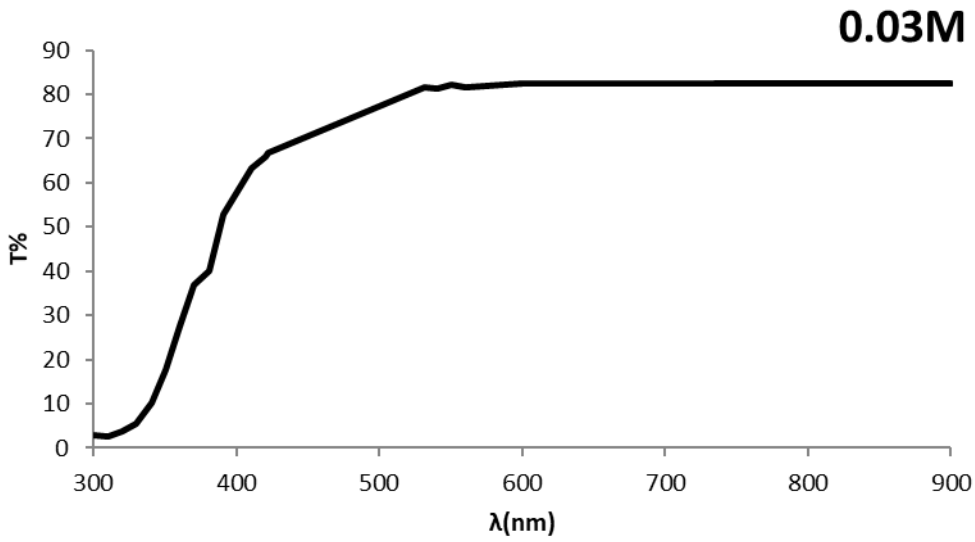

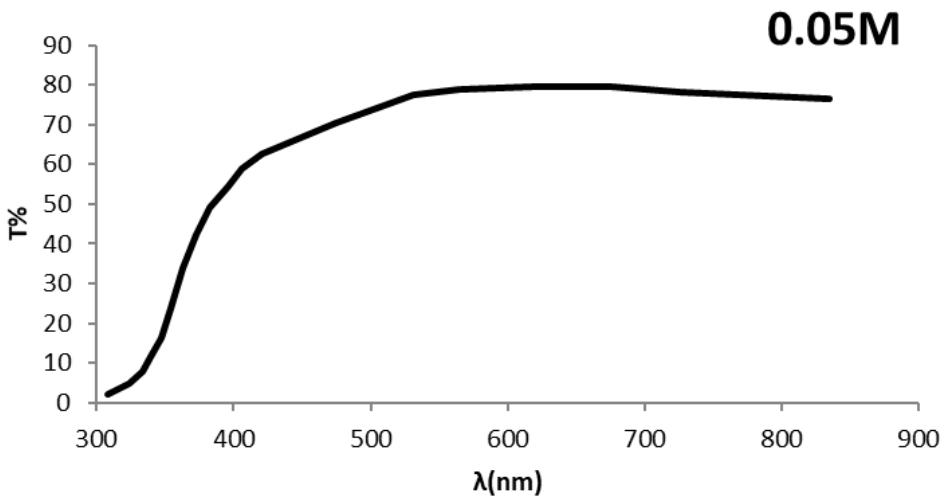

Figure 2: Transmittance spectra of prepared MoO3 thin films

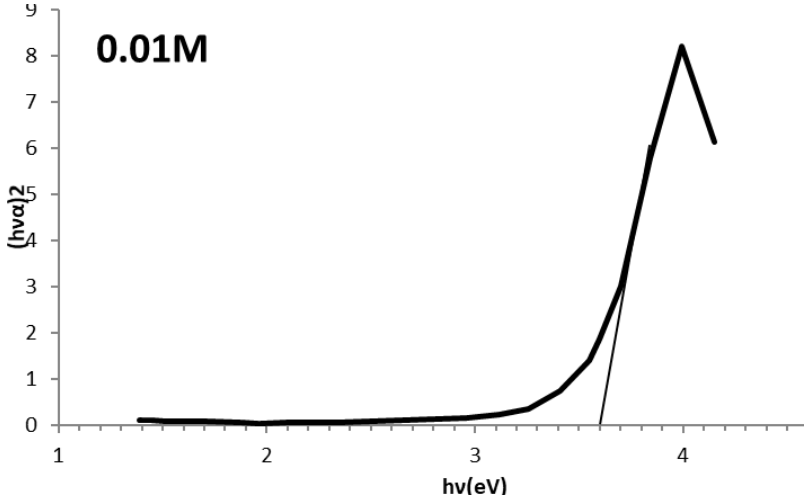

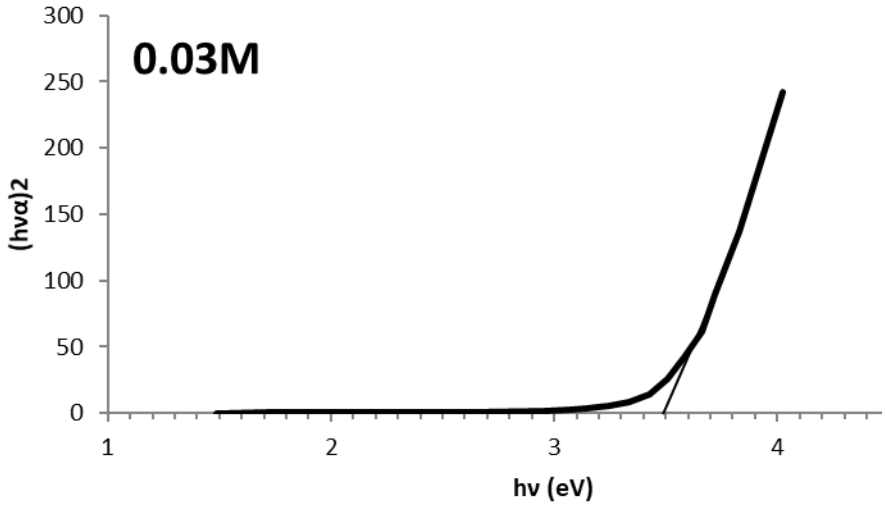

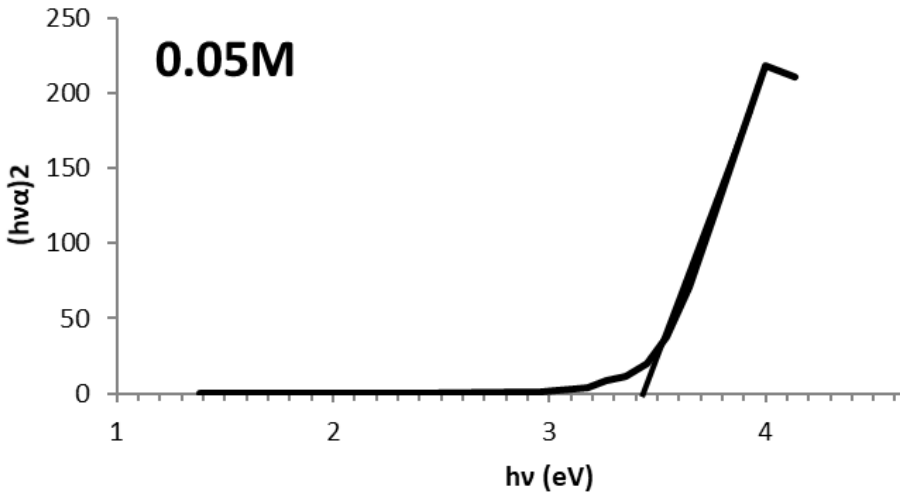

Figure 3: Tauc plot of prepared MoO3 thin films

Table 3: Optical Parameters Summary

Concentration (M)	T (400–800 nm) (%)	Max T (nm)	Eg (eV)
0.01 (Amorphous)	87	600	3.6
0.03	78	550	3.5
0.05 (Crystalline)	82	550	3.4

Enhanced grain growth at higher concentrations reduces grain boundary scattering (improving T) while increasing α via momentum-conserving transitions. Eg narrowing follows Burstein-Moss shift reversal as defect states fill and conduction band effective mass decreases in larger crystallites. High T in amorphous films results from index matching with substrate, but lacks sharp absorption edge. 0.05 M films optimize T>80% with Eg ≈ 3.0 eV perfect band alignment for hole transport layers (HIL) in OLEDs/PLEDs and buffer layers in solar cells. Interference fringes confirm uniform thickness, essential for reproducible device fabrication. Thus, 0.05 M delivers optimal balance of high visible transparency, strong UV absorption, and narrowed band gap matching literature values for high-quality α-MoO_3. Lower concentrations sacrifice absorption strength; higher risks opacity from aggregation. These results validate spray pyrolysis at 0.05 M as industrially-viable for transparent conductors and energy devices requiring >80% transmittance with >3 eV band gap [12-13].

4. CONCLUSION

This study demonstrates that precursor concentration critically governs the structural and optical evolution of spray-pyrolyzed MoO_3 thin films at fixed 200°C. Low concentrations yield amorphous structures with broad XRD humps, transitioning to highly crystalline orthorhombic α-MoO_3 featuring characteristic Bragg reflections matching JCPDS standards. Scherrer and Williamson-Hall analyses confirm systematic crystallinity enhancement through increased nucleation density and grain growth, while compressive microstrain reflects epitaxial substrate interactions. UV-Vis spectroscopy reveals corresponding optical optimization: crystalline films achieve high visible transmittance, sharp UV absorption edges, and narrowed direct band gap via delocalization and defect passivation. These definitive structure-property correlations establish optimal processing conditions delivering device-ready films with balanced nanostructure, transparency, and wide band gap—ideal for electrochromic devices, gas sensors, and photovoltaics. Spray pyrolysis's vacuum-free scalability positions it as an industrially viable route for large-area transition metal oxide thin films through rational concentration engineering.

5. REFERENCES

1. Granqvist CG. Handbook of Inorganic Electrochromic Materials. Elsevier; 1995.
2. Comini E, et al. Sens. Actuators B. 2009;140:16-27.
3. Meyer J, et al. Adv. Mater. 2012; 24:1844-1852.
4. Patil PS. Appl. Surf. Sci. 1999; 153:126-140.
5. Bouzidi A, et al. Mater. Sci. Eng. B. 2004; 109:68-73.
6. Choudhuri A, et al. Thin Solid Films. 2015; 595:102-109.
7. Karuppasamy A, et al. Ceram. Int. 2016; 42:17385-17395.
8. Deepa M, et al. Sol. Energy Mater. Sol. Cells. 2006; 90:2540-2554.
9. Chernyak L, et al. J. Phys. Chem. C. 2014;118:9498-9504.
10. Rakhshani SA. J. Appl. Phys. 1997; 81:1846-1851.

11. Vijayakumar A, et al. Ionics. 2012; 18:293-298.
12. Gesztler M, et al. Sol. Energy Mater. Sol. Cells. 2018; 178:236-243.
13. Lewis NS, et al. MRS Bull. 2017; 42:880-887.